Mechanical behavior of a ferritic stainless steel under simple and complex loading paths

B. Rossi & J.-P. Jaspart
University of Liège, Liège, Belgium

ABSTRACT: For what regards the cost difference between carbon and stainless steels, ferritic grades are often cited as a possible competitive solution. Nevertheless, little information specifically dedicated to this material is available, limiting its use in innovative structures. In this paper, the selected stainless steel grade 1.4003 commonly called 3Cr12 is considered. In order to improve the comprehension of this material, an extensive characterization of its mechanical behavior is performed using uniaxial tensile and shear tests combined with biaxial tests such as successive shear and tensile tests. Cold-rolled sheets are used for the tests and the results of the study are related to cold-formed lightweight structures. The subsequent experimental results enable the identification of several models such as the very complete Teodosiu-Hu's microstructural based hardening model. Other traditional constitutive models are also characterized: Armstrong-Frederick and Ramberg-Osgood. The models predictions are found to be accurate with respect to the test results.

1 INTRODUCTION

Ferritic stainless steels are corrosion resistant steels with a low and stable cost. Widely used in automotive exhaust systems, automotive trim, hot water tanks, fuel lines, cooking utensils or structural parts in coach structures, structural applications using ferritic stainless steels are only emerging mainly because ferritics are partially covered by structural standards due to a shortage of design data. Indeed, little information specifically dedicated to ferritic grades is available in the literature whereas austenitic grades are much more covered (Gardner 2002, Ashraf 2006, Lecce 2006, Cruise 2007). Computer models are extensively used to support the developments of conventional design methods based on expensive full-scale tests or trial and errors methods. And for the modeling of the structural response of members, it is necessary to afford an accurate knowledge of the mechanical properties. The material behavior is inseparable of the structural response of stainless steel members as it has been abundantly illustrated over the past few years: authors such as Rasmussen and Rondal (Rasmussen & Rondal 1997, 2000), Rondal and Rasmussen (Rondal & Rasmussen 2000), Nethercot and Gardner (Nethercot & Gardner 2004), Gardner and Nethercot (Gardner & Nethercot 2004a,b), Gardner and Ashraf (Gardner & Ashraf 2006) and Rossi et al. (Rossi 2008, Rossi et al. 2009a,b) studied the effect of the non-linear stress-strain behavior on member capacity.

In this paper, the experimental investigations made on the chromium based alloy 3Cr12 (1.4003) in order to characterize its mechanical behavior are presented. During the research, classical uniaxial experimental equipment and biaxial experimental equipment designed by Flores (Flores 2005) in the Structures Laboratory of the University of Liège have been used. The collection of tests performed included tensile tests, cyclic shear tests, simple shear tests and successive simple shear and plane-strain tests. The yield locus and the hardening models are then presented and the parameters included in each law are carefully identified.

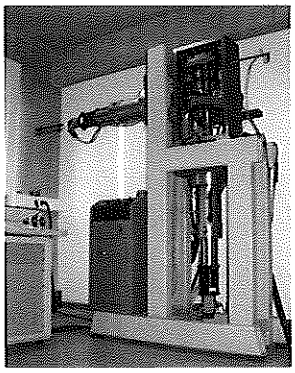

Figure 1. Biaxial experimental equipment developed at the Structures Laboratory of the University of Liège

2 EXPERIMENTAL INVESTIGATIONS

2.1 *Type of tests*

Cold-rolled sheets are used for the tests and the results of the study are related to cold-formed lightweight structures. The characterization of the material behavior requires several types of tests in the rolling direction (RD, $\alpha = 0°$), transverse direction (TD, $\alpha = 90°$) and at 45° from the rolling direction, including: (1) uniaxial tensile coupon tests (UTT) and plane strain tensile tests (PST); (2) uniaxial simple shear (SST) and biaxial simple shear tests (Bauschinger tests, BT); (3) biaxial tests, combining successive tension and shear (orthogonal tests, OT).

2.2 *Uniaxial tensile tests*

The tensile tests are performed in a classical electro-mechanical tensile test machine. The capacity of the mechanical grips is 20 kN. Strain gauges (rosettes, strain measure capacity up to 5%), placed at both sides of the sample, are used to measure the strain for the identification of the elastic parameters (E0, ν) and the determination of the yield limit.

2.3 *Biaxial tests*

The equipment developed by Flores (Flores 2005) in the Structures Laboratory of the University of Liège is composed of two hydraulic jacks controlled simultaneously in displacements and forces. In Figure 1, the black arrows show the possible movements of the device: vertical and horizontal displacements of the jacks are possible successively or simultaneously. The sample is clamped between two grips. The geometry of the grip limits the specimen's thickness to 1.6mm. The device allows the user to perform PST, SST as well as successive or simultaneous simple shear tests and plane strain tests. The data acquisition system called Aramis® is able to record the applied loads, the displacements of the grips and the strain field over the tested sample.

2.4 *Tests results*

Concerning the UTT, the PST and the SST, three identical tests have been realized for each of the three directions. Consequently, a set of 27 tests has been conducted. They allow identifying, amongst other things, the material anisotropy. Moreover, BT at three levels of pre-straining and OT at two levels of pre-straining have been realized in the RD. Therefore, a second set of 15 tests have been conducted.
The stress-strain curves for UTT, PST and OT, BT appear in Figure 2.

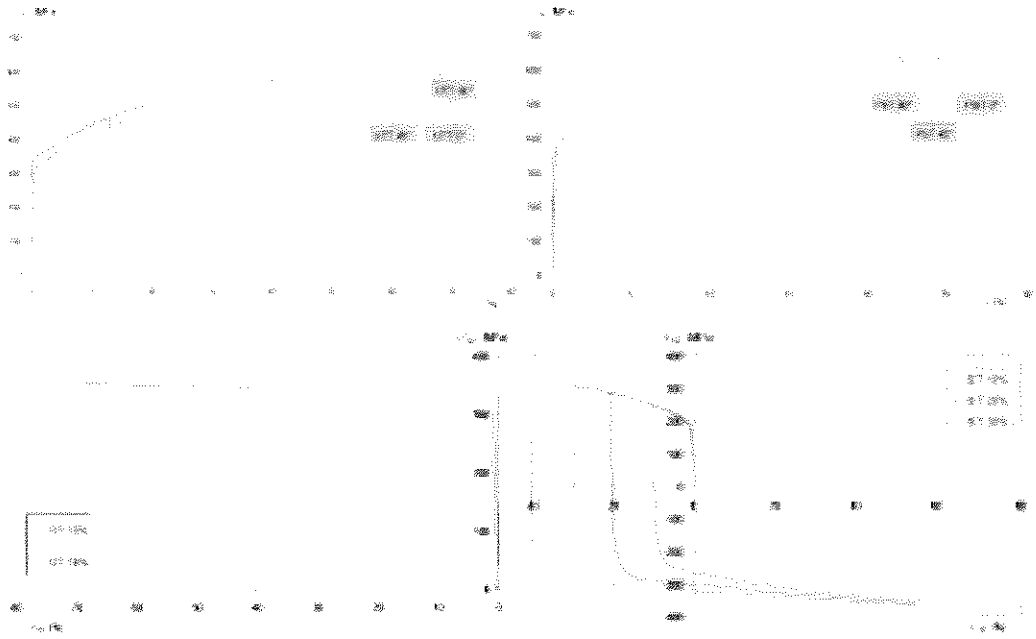

Figure 2. Uniaxial and biaxial tests: True-stress - natural strain curves

Table 1. Initial yield stresses.

Tests	Experimental Point	Measured stresses
		MPa
UTT RD	$\sigma_{exp,1} = \sigma_{11}$	315,21
UTT TD	$\sigma_{exp,2} = \sigma_{11}$	342,60
UTT 45°	$\sigma_{exp,3} = \sigma_{11}$	348,33
PST RD	$\sigma_{exp,4} = \sigma_{11}$	343,10
PST TD	$\sigma_{exp,5} = \sigma_{11}$	343,51
PST 45°	$\sigma_{exp,6} = \sigma_{11}$	375,01
SST RD	$\sigma_{exp,7} = \sigma_{12}$	179,47
SST 45°	$\sigma_{exp,8} = \sigma_{12}$	173,65

The initial yield stresses for each stress state are the ones providing the same plastic work W_{0p} as the one corresponding to the uniaxial tensile test in the RD, they are reported in Table 1. Anisotropic materials will show a variation of the yield stress with the orientation angle α.
The Lankford coefficient is the ratio between the plastic strain rate in the width direction and in the thickness direction. Typically, Lankford coefficients for rolled metals will be sensitive to the loading direction (along RD, TD and at at 45° from the RD). The coefficients are deduced from the strain measurements obtained from UTT performed at different angles α from the RD. If the Lankford coefficients are evaluated when 0.2% of plastic strain is reached, the following values are obtained:

- $r_{0,exp} = r_{exp,1} = 0,83$;
- $r_{90,exp} = r_{exp,2} = 0,85$;
- $r_{45,exp} = r_{exp,3} = 0,79$.

The average Lankford coefficient's value (called coefficient of normal anisotropy) $\bar{r}$ is $(r_0 + 2.r_{45} + r_{90}) = 0.82$. Low $\bar{r}$ values have been related to less drawability in steel sheets. The interested reader can refer to (Rossi 2008) for further information.

3 YIELD LOCUS AND HARDENING LAWS

3.1 *Introduction*

Although no significant kinematic hardening response is observed, the observed material stress-strain properties will be modeled using isotropic and combined isotropic-kinematic hardening models. The influence of the amount of pre-strain on the flow stress stagnation (WHS) after reversing the load and the increase of the yield stress after an orthogonal strain-path change (RTR) can be underlined using the biaxial tests and it is possible to model such effects using micro-macro hardening models. The anisotropy, initial yield locus and hardening behavior are characterized on the basis of an optimization procedure described in (Flores 2005, Rossi 2008). For the identification of the yield locus equation (Hill's 1948 yield locus), three different methods have been investigated: (1) the first one uses the Lankford coefficients, (2) the second one uses the yield stresses, (3) the last one combines yield stresses and Lankford coefficients. The results of the last one will be presented herein. Afterwards, the experimental curves, exempt of any measurement perturbation, will be used to optimize the material parameters included in each investigated law. Such experimental results provide the necessary data to identify the material parameters included in models such as the ones suggested by Ramberg-Osgood (Rasmussen 2003) and Armstrong-Frederick (Armstrong & Frederick 1966) or more complex ones like the Teodosiu-Hu model (Teodosiu & Hu 1997). These parameters are adjusted in order to minimize an error function established between the experimental and the theoretical curves. For Teodosiu-Hu law, it will be necessary to perform the optimization with the help of the optimization code Optim coupled with the finite element code Lagamine both developed at the University of Liège.

3.2 *Elastic behavior*

The Young's modulus and Poisson's ratio are determined from the uniaxial tensile tests at different angles from the RD. Three tests were performed for each direction and two different devices (displacements transducers and strain gauges) have been used to measure the strain. Two measures of the Young's modulus have been recorded at both sides of the sample. The average values of E_0 and ν are found respectively equal to $E_0 = 178$GPa and $\nu = 0.298$.

3.3 *Hill's 1948 yield locus*

In Hill's 1948 criterion, F, G, H, N, L and M are material parameters that describe the material orthotropy:

$$2\bar{\sigma}^2 = H(\sigma_{11}-\sigma_{22})^2 + G(\sigma_{11}-\sigma_{33})^2 + F(\sigma_{22}-\sigma_{33})^2 + 2N\sigma_{12}^2 + 2L\sigma_{13}^2 + 2M\sigma_{23}^2 = 2\sigma_y^2 \qquad (1)$$

where $\bar{\sigma}$ = equivalent stress; σ_y = yield stress.

Firstly, assuming Hill's 1948 criterion, a general expression relating σ_{11} or σ_{12} with $\sigma_y = \sigma_{exp,i}$ can be established for each stress state (Flores 2005). Those theoretical expressions, dependant on the material parameters F, G, H and N, can be compared to the experimental values $\sigma_{exp,i}$ for each test.
Secondly, the Lankford coefficients can be linked to the material parameters included in the yield surface equation using the associated plasticity theory and these theoretical expressions can also be compared to the experimental values of $r_{exp,i}$.
The method consists in optimizing the material parameters of Hill's 1948 yield criterion in order to minimize an error function established between the experimental and the theoretical yield stress and Lankford coefficients:

$$\chi = \sum_{i=1,l}(1-\eta)\left[\frac{\sigma_{theo,i}-\sigma_{exp,i}}{\sigma_y}\right]^2 + \sum_{j=1,m}\eta\left[\frac{r_{theo,j}-r_{exp,j}}{\bar{r}}\right]^2 \qquad (2)$$

where $\bar{r}$ = coefficient of normal anisotropy; l = number of tests performed to measure the yield stress; m = number of tests used to define the Lankford coefficients; η weights the influence of the stress measurements and the strain measurements.

Table 2. Parameters F, G, H and N for Hill's 1948 yield locus.

η	F	G	H	N
1	1,1439	1,0936	0,906	3,014

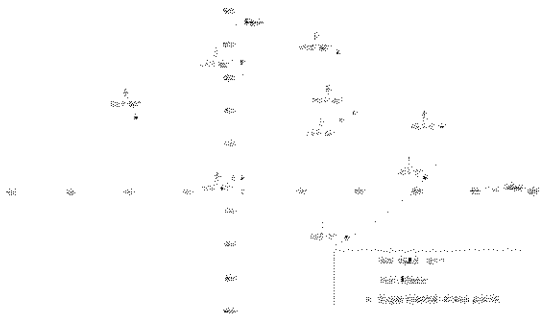

Figure 3. Contours of equivalent plastic work, von Mises and Hill's 1948 yield loci (F, G, H, N from Table 2)

Table 3. Average material parameters for Ramberg-Osgood law.

E_0	$\sigma_{0.2}$	$\sigma_{0.01}$	n	E_2	e	ε_u	σ_u	m	$\varepsilon_{0.2}$
MPa	MPa	MPa		MPa			MPa		
180510	337	269	13,5	11828	0,0019	0,286	614	1,97	0,0034

After all calculations, it is seen that Hill's 1948 yield locus using $\sigma_{exp,1}$ for the yield stress provides the most accurate results. Among the fitted Hill's yield loci, it is interesting to note that the case η=1 (Lankford coefficient method, results in Table 2) renders the most satisfying results. All the corresponding curves can be found in (Rossi 2008).
Figure 3 represents the experimental results in stress space (σ_{11}, σ_{22}) together with the yield locus. Indeed: (1) uniaxial tensile tests performed in the RD, the TD and at 45° from the RD allow to identify three points (1, 2 and 3); (2) large tensile tests provide three additional points (4, 5 and 6) and (3) at small strains, a simple shear test can be used to approximate a pure shear state and therefore three additional reference points (7, 8 and 9) can be plotted in the stress space (σ_{11}, σ_{22}, σ_{12}).

3.4 *Modified Ramberg-Osgood's type isotropic hardening*

The modified Ramberg-Osgood law contains 6 parameters: the initial Young's modulus E_0, the proof stress $\sigma_{0.2}$ corresponding to an equivalent plastic strain offset of 0.2%, the ultimate stress σ_u and ultimate deformation ε_u and finally the parameters n and m characterizing the roundness of the non linear stress-strain relationship. All the equations describing the hardening model can be found in (Rasmussen 2003). The material parameters are dependant on the chosen curves for the identification. In the present research, UTT have been used for the identification. The average parameters appear in Table 3. The parameter n plays an important role when calculating the resistance of members as shown in (Rossi et al. 2009a,b).

3.5 *Armstrong-Frederick's type kinematic hardening and Teodosiu-Hu's type micro-structural based hardening*

Kinematic hardening can predict the Bauschinger effect appearing after a reversed loading using a second order back stress tensor $\underline{X}$ that describes the movement of the center of the yield surface due to plastic strain. The difference between Armstrong-Frederick and Teodosiu-Hu model lay in the number of material parameters included in the laws and, inevitably, in their accuracy

to describe the phenomenon. Teodosiu-Hu is based on microscopic and macroscopic experimental observations and can predict: (1) the macroscopic anisotropic behavior such as the Bauschinger effect; (2) the observed work-hardening stagnation under reversed deformation at large strains (WHS) and (3) the work-softening during a subsequent orthogonal deformation (RTR). But the model contains 13 parameters to be optimized using UTT, SST, BT and OT. This requires the use of an optimization tool, herein the optimization code Optim coupled with the finite element code Lagamine. If coupled with the isotropic Swift's hardening (Rossi 2008), Armstrong-Frederick only contains five parameters but the precision of the model is poorer in this case. All the equations describing the hardening model can be found in (Rossi 2008). In (Flores 2005), the author set up a procedure to find the set of material parameters included in Armstrong-Frederick and Teodosiu-Hu's hardening laws. Flores studied the influence of each parameter on the stress-strain curves and proposed to progressively optimize the set of parameters according to his conclusions. In the present research, the application of this procedure provides the results of Table 4.

Table 4. Material parameters for the combined hardening law (Swift and Armstrong-Frederick laws) and the micro-structural based Teodosiu-Hu hardening law.

K	ε_0		n	C_X	X_{SAT}							
MPa					MPa							
598,99	0,0214		0,373	323,02	98,76							
m	R_0	C_R	R_{SAT}	C_X	X_{SAT0}	q	C_{SD}	C_{SL}	S_{SAT0}	n_P	n_L	C_P
	MPa		MPa		MPa				MPa			
0,175	307,5	17,14	6,40	295,7	191,2	2,86	8,94	4,62	381,7	23,3	10^{-7}	8,8

If Armstrong-Frederick hardening model is utilized, the results are shown in Figure 4. For the good comprehension of the reader, it is interesting to underline that, for computational reason, the negative part of the curves in the BT are reported in the right superior quadrant.

If Teodosiu-Hu hardening model is utilized, the comparisons between the experimental and theoretical stress-strain curves appear in Figure 5.

4 CONCLUSIONS

This paper presents the experimental and theoretical investigations performed to characterize the mechanical behavior of the 1.4003 stainless steel grade. The material behavior is characterized by performing several types of tests on samples cut out of the delivered sheet in the RD, TD and at 45° from the RD: (1) uniaxial tensile coupon tests and plane strain tensile tests; (2) uniaxial and biaxial simple shear tests and (3) biaxial tests, combining tension and shear. In total, more than 40 tests have been performed. A general constitutive equation is defined using the classical concepts of plasticity theory such as yield function, plastic flow rule and hardening constitutive laws. The study focuses on the identification of yield functions modeling the material anisotropy as well as hardening constitutive laws able to predict strain-induced anisotropy. But other classical hardening laws as the isotropic Ramberg-Osgood's and the kinematic Armstrong-Frederick's hardening models are also studied. Firstly, the elastic parameters are identified using uniaxial tensile tests. Secondly, the yield surface equation is defined using two types of experimental results: (1) the Lankford coefficients that are computed from strain data measured during the UTT and (2) the yield stress points that are calculated from each different stress state. These points define the contours of equivalent plastic work. Both von Mises and Hill's 1948 yield loci can model the experimental data with little discrepancies. Afterwards, the different stress-strain curves are used to define the hardening constitutive laws. Isotropic hardening laws such as Ramberg-Osgood's one are first studied.

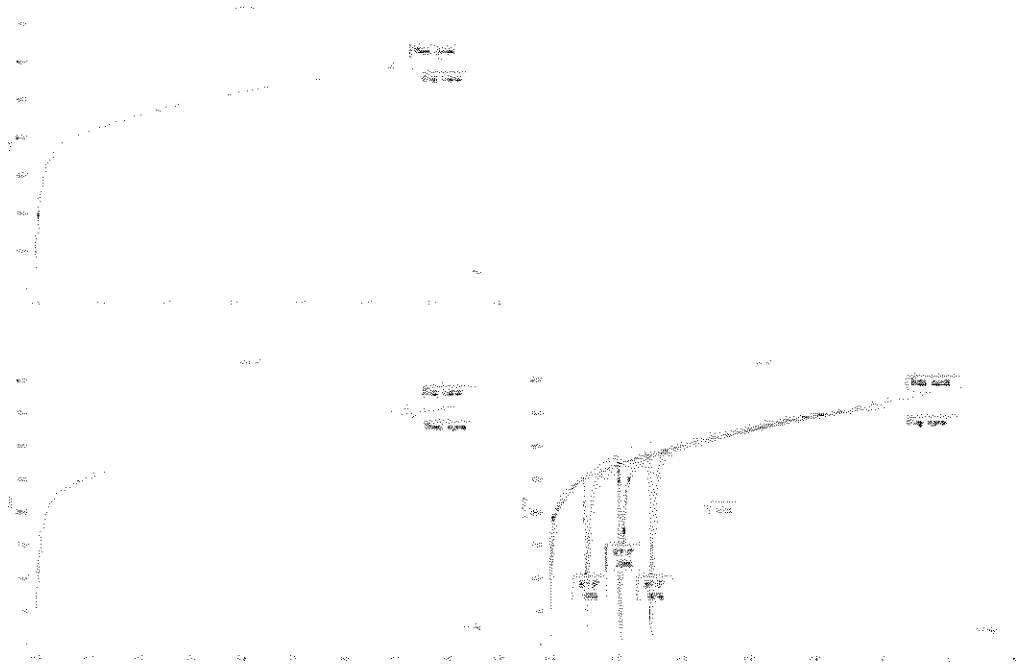

Figure 4. UTT, SST and BT: True-stress - natural strain curves, Armstrong-Frederick hardening model

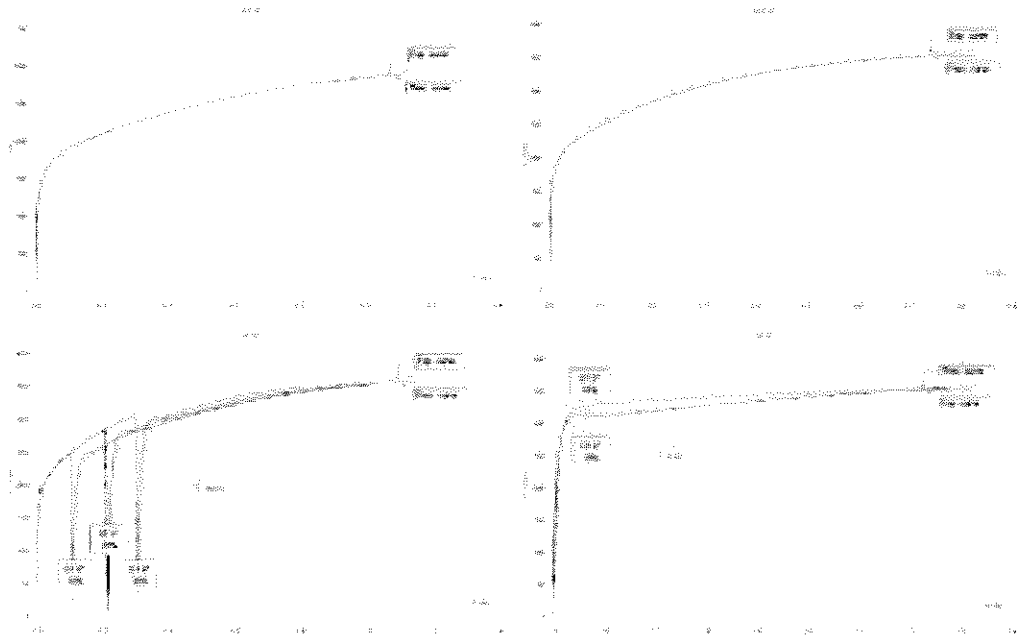

Figure 5. UTT, SST, BT and OT: True-stress - natural strain curves, Teodosiu-Hu hardening model

Even if relatively low kinematic hardening behavior is observed, the parameters for the Armstrong-Frederick's kinematic hardening are also characterized. And last, the micro-macro Teodosiu-Hu's hardening law is studied. In this case, the optimized set of parameters is able to describe the flow stress behavior after the strain-path change in the case of cyclic shear tests and pre-strained shear tests (orthogonal tests). Armstrong-Frederick's and Teodosiu-Hu's hardening laws are identified with an optimization procedure using the optimization code Optim based on the main Levenberg algorithm and the finite element code Lagamine. During the optimization,

the tests results and the finite element simulations of the tests are compared and the material parameters are adjusted in order to best fit the experimental curves.

The choice of the laws and the best set of parameters requires all the user's expertise and depends on the considered application. For instance, in the case of deep drawing, the final shape of the product strongly depends on the plastic behavior of the material and complex constitutive models provide better results (Flores et al. 2007). Authors (Gardner & Nethercot 2004b, Lecce 2006, Rossi 2008) also showed that the structural response using numerical analysis fails to properly model the behavior of stainless steel members if the material behavior is not well taken into account, careful consideration must be brought to the evaluation of the material parameters. Indeed, the modified Ramberg-Osgood's law seems well-adapted for the modeling of stainless steels and in (Rossi 2009a,b), it is underlined that the material parameters, especially the parameter n included in Ramberg-Osgood's law, play an important role in the theoretical evaluation of the carrying capacity of stainless steel columns.

5 REFERENCES

Armstrong, P. J. & Frederick, C. O. (Berkeley Nuclear Laboratories) 1966. *A mathematical representation of the multiaxial Bauschinger effect. GEGB Report RD/B/N731.*

Ashraf, M. 2006. *Structural stainless steel design: resistance based on deformation capacity.* London, Imperial College London.

Cruise, R. 2007. *The influence of production routes on the behavior of stainless steel structural members.* London, Imperial College London.

Flores, P. 2005. *Development of experimental equipment and identification procedures for sheet metal constitutive laws.* Liège, University of Liège.

Flores, P. & Duchêne, L. & Bouffioux, C. & Lelotte, T. & Henrard, C. & Pernin, N. & Van Bael, A. & He, S. & Duflou J. & Habraken, A.-M. 2007. Model identification and FE simulations: Effect of different yield loci and hardening laws in sheet forming. *International Journal of Plasticity*, 23(3):420–449.

Gardner, L. 2002. *A new approach to stainless steel structural design.* London, Imperial College London.

Gardner, L. & Nethercot, D. A. 2004. Structural stainless steel design: a new approach. *The Structural Engineer.* 82:21–30.

Gardner, L. & Nethercot, D. A. 2004. Numerical modeling of stainless steel structural components - a consistent approach. *Journal of Structural Engineering*, 130(10):1586–1601.

Gardner, L. & Ashraf, M. 2006. Structural design for non-linear metallic materials. *Engineering Structures*, 28(6):926–934.

Lecce, M. 2006. *Distortional buckling of stainless steel sections.* Sydney, The University of Sydney.

Nethercot, D. A. & Gardner, L. 2004. Exploiting the special features of stainless steel in structural design. *Applied Mechanics and Engineering.* 8:7–24.

Rasmussen, K. J. R. & Rondal, J. 1997. Strength curves for metal columns. *Journal of Structural Engineering*, 123(6):721–728.

Rasmussen, K. J. R. & Rondal, J. 2000. Column curves for stainless steel alloys. *Journal of Constructional Steel Research.* 54(1):89–107.

Rasmussen, K. J. R. 2003. Full-range stress-strain curves for stainless steel alloys. *Journal of Constructional Steel Research*, 59(1):47–61.

Rondal, J. & Rasmussen, K. J. R. 2000. Strength curves for aluminium alloy columns. *Engineering Structures.* 22(11):1505–1517.

Rossi, B. 2008. *Mechanical properties, residual stresses and structural behavior of thin-walled stainless steel profiles.* Liège, University of Liège.

Rossi, B. & Jaspart J. P. & Rasmussen. K. J. R. 2009. Combined distortional and overall flexural-torsional buckling of cold-formed stainless steel sections: Experimental investigations. *Journal of the Structural Engineering-Asce*, In press, april 2010.

Rossi, B. & Jaspart J. P. & Rasmussen. K. J. R. 2009. Combined distortional and overall flexural-torsional buckling of cold-formed stainless steel sections: Design. *Journal of the Structural Engineering-Asce,* In press, april 2010.

Teodosiu, C. & Hu, Z. 1997. Evolution of the intragranular microstructure at moderate and large strains: modeling and computational significance. *Simulation of Material Processing: Theory, Methods and Applications*, 173–182.